Cell Calcium 96 (2021) 102390

Contents lists available at ScienceDirect

Cell Calcium

journal homepage: www.elsevier.com/locate/ceca

Enhanced modulation of cell-type specific neuronal responses in mouse dorsal auditory field during locomotion

Julia U. Henschke [a,b], Alan T. Price [a,b,c], Janelle M.P. Pakan [a,b,d,*]

[a] Institute of Cognitive Neurology and Dementia Research, Otto-von-Guericke-University Magdeburg, Leipziger Str. 44, 39120, Magdeburg, Germany
[b] German Centre for Neurodegenerative Diseases, Leipziger Str. 44, 39120, Magdeburg, Germany
[c] Cognitive Neurophysiology group, Leibniz Institute for Neurobiology (LIN), 39118, Magdeburg, Germany
[d] Center for Behavioral Brain Sciences, Universitätsplatz 2, 39120, Magdeburg, Germany

ARTICLE INFO

Keywords:
Auditory cortex
Dorsal auditory field
Two-photon calcium imaging
Interneurons
Locomotion
Sensory-evoked responses

ABSTRACT

As we move through the environment we experience constantly changing sensory input that must be merged with our ongoing motor behaviors - creating dynamic interactions between our sensory and motor systems. Active behaviors such as locomotion generally increase the sensory-evoked neuronal activity in visual and somatosensory cortices, but evidence suggests that locomotion largely suppresses neuronal responses in the auditory cortex. However, whether this effect is ubiquitous across different anatomical regions of the auditory cortex is largely unknown. In mice, auditory association fields such as the dorsal auditory cortex (AuD), have been shown to have different physiological response properties, protein expression patterns, and cortical as well as subcortical connections, in comparison to primary auditory regions (A1) - suggesting there may be important functional differences. Here we examined locomotion-related modulation of neuronal activity in cortical layers $^{2}/_{3}$ of AuD and A1 using two-photon Ca^{2+} imaging in head-fixed behaving mice that are able to freely run on a spherical treadmill. We determined the proportion of neurons in these two auditory regions that show enhanced and suppressed sensory-evoked responses during locomotion and quantified the depth of modulation. We found that A1 shows more suppression and AuD more enhanced responses during locomotion periods. We further revealed differences in the circuitry between these auditory regions and motor cortex, and found that AuD is more highly connected to motor cortical regions. Finally, we compared the cell-type specific locomotion-evoked modulation of responses in AuD and found that, while subpopulations of PV-expressing interneurons showed heterogeneous responses, the population in general was largely suppressed during locomotion, while excitatory population responses were generally enhanced in AuD. Therefore, neurons in primary and dorsal auditory fields have distinct response properties, with dorsal regions exhibiting enhanced activity in response to movement. This functional distinction may be important for auditory processing during navigation and acoustically guided behavior.

1. Introduction

Our perception of the surrounding environment is driven by constantly changing sensory inputs that are, in turn, substantially influenced by motor behaviors. Evidence from a wide variety of sensory systems indicates sensory processing may be directly modulated during self-motion using corollary discharge from a motor command signal; ultimately facilitating sensory-guided behaviors [1,2]. This highlights the importance of investigating the effects of motor behaviors on sensory processing in vivo and in awake behaving animals [3–6]. Substantial evidence has shown that locomotion-responsive neurons in both primary visual cortex [7–9] and somatosensory cortex [10,11], result in a general enhancement of activity and a gain in sensory-evoked neuronal responses during locomotion. In contrast, there is evidence that locomotion largely suppresses neuronal responses in layer $^{2}/_{3}$ in auditory cortex [12–15]; supporting a theory that responses to self-generated and non-relevant sounds are dampened as an animal moves through an environment [16,17]. This has been proposed to act through fast-spiking interneurons expressing parvalbumin (PV) [12–14,16]. Importantly, previous studies have not always specified the precise anatomical location of these response dynamics within the auditory cortex; hence, it is unknown whether neurons in higher-order auditory

* Corresponding author at: Institute of Cognitive Neurology and Dementia Research, Otto-von-Guericke University, Magdeburg, 39120, Germany.
E-mail address: janelle.pakan@med.ovgu.de (J.M.P. Pakan).

https://doi.org/10.1016/j.ceca.2021.102390
Received 29 January 2021; Received in revised form 5 March 2021; Accepted 10 March 2021
Available online 17 March 2021

fields are modulated by locomotion in the same way as A1.

In mice, neurons in auditory association fields, such as the dorsal auditory cortex (AuD), have been shown to have different physiological response properties (e.g. broader frequency tuning and non-tonotopic organization [18], protein expression patterns (calcium-binding proteins such as PV and calbindin [19,20] and non-phosphorylated neurofilaments [21]; also observed in gerbils [22], as well as thalamic [23], subcortical [24,25] and cortical [20,26,27] connections, in comparison to A1. There is also some evidence from large-scale connectome data that dorsal auditory regions are more connected with motor cortex [26,27], however, the details remain unclear. In addition, we have recently shown that AuD is linked with the cerebellum, a major center for motor control and associative learning, via a direct cortico-pontine-cerebellar pathway, whereas cerebrocerebellar pathways originating from A1 are more polysynaptic involving collicular and vestibular nuclei as intermediaries [24]. Therefore, it is possible that AuD may be responsive to more motor-dependent information, including responses related to self-motion; however, the effects of locomotion in AuD and its role in motor-related and sensory-evoked auditory processing remains unknown.

Here we examine locomotion-related modulation of neuronal activity in cortical layers $^{2}/_{3}$ of AuD and A1 using two-photon Ca^{2+} imaging in head-fixed behaving mice that are able to freely run on a spherical treadmill. We determine the proportion of neurons in these two auditory regions that show enhanced and suppressed sensory-evoked responses during locomotion and quantify the depth of modulation. We further detail differences in the circuitry between these auditory regions and the motor cortex, and show that AuD is more highly connected to motor cortical regions. Finally, we compare the cell-type specific locomotion-evoked modulation of responses in AuD.

2. Materials and methods

2.1. Animals

Experiments were performed across 40 imaging sessions (19 mice, 9–12 weeks; both males and females); 4 C57BL/6 J wildtype mice (RRID: IMSR_JAX:000664; Jackson Laboratory), 11 GCaMP6f (C57BL/6 J-Tg(Thy1-GCaMP6f)GP5.5Dkim/J; RRID: IMSR_JAX:024276), 2 PV.cre (B6;129P2-Pvalb$^{tm1(cre)Arbr}$/J; RRID: IMSR_JAX:008069) and 2 Ai9 tdTomato reporter mice (B6.Cg-Gt(ROSA)26Sor$^{tm9(CAG-tdTomato)Hze}$/J; RRID: IMSR _JAX:007909). Mice were housed in standard cages at a 12 h/12 h light dark cycle, food and water were provided ad libitum. All experiments were performed according to the NIH Guide for the Care and Use of Laboratory animals (2011) and the Directive of the European Communities Parliament and Council on the protection of animals used for scientific purposes (2010/63/EU) and were approved by the animal care committee of Sachsen-Anhalt, Germany (42502-2-1479 DZNE).

2.2. Surgery

2.2.1. Cranial window

For cranial window implantation and virus injection, all mice were anaesthetized with isoflurane (4% for induction and 2% maintenance during surgery). Eye cream was applied to protect the eyes (Bepanthen, Bayer), analgesics and anti-inflammatory drugs were injected subcutaneously (carprofen, 0.15 mg, and dexamethasone, 2 mg). After shaving and disinfection of the head skin, a section of the scalp was removed. A craniotomy was then made over the left auditory cortex, the window was approximately 1.5 × 3 mm for AuD and 1.5 × 1.5 mm for A1. For calcium imaging in wildtype mice an adeno-associated virus (AAV) was injected (AAV1.Syn.GCaMP6m.WPRE.SV40; RRID: Addgene_100841) and in PV.cre mice (AAV1.Syn.Flex.GCaMP6m.WPRE.SV40; RRID: Addgene_100838). Injections were made with a Nanoject (World Precision Instruments, Germany) and a glass pipette with ~20 μm tip diameter at depths throughout the cortex (ranging 250−600 μm deep; in 20 × 10 nl steps), injecting at a slow speed of 10 nl min-1 to limit tissue damage. For all animals, a glass coverslip was then placed on top of the craniotomy and fixed with glue (gel control, Loctite). A custom-built headplate was implanted on the exposed skull with glue and cemented with dental acrylic (Paladur, Heraeus Kulzer). After recovery from anesthesia, animals with AAV injections were returned to their home cage, for 2–3 weeks to allow for virus expression and clearing of the cranial window before imaging (see also [28]). For transgenic CGaMP6 mice, acute imaging started 24 h after recovery from surgery and continued after 2–3 weeks once the cranial window had cleared.

2.2.2. Transsynaptic tracer injections

To investigate the pathway from motor cortex to auditory cortices we injected a mono-trans-synaptic adeno-associated virus (AAV1.cre; AAV1.hSyn.Cre.WPRE.hGH, Addgene, USA, RRID: Addgene_105553) in two tdTomato expressing Ai9 reporter mice. This AAV1.cre virus drives expression of cre, which results in tdTomato expression in individual neurons using the Ai9 reporter mouse line. The AAV1.cre is transported anterogradely to mono-synaptically connected neurons [29–31] and subsequently also drives cre expression in target neurons in connected brain regions; tdTomato reporter expression then fills these target neurons [30]. This AAV1.cre construct has been shown to spread exclusively to synaptically connected neurons with trans-synaptic spread nearly abolished by tetanus toxin light chain (i.e. inhibition of presynaptic vesicle fusion [31]). Limitations in transport may exist through neuromodulatory projections (e.g. noradrenergic, cholinergic, serotonergic), however, efficient transport has been demonstrated for glutamatergic and GABAergic synapses to both excitatory and inhibitory neurons as well as long-distance projections [31]. Low efficiency retrograde transport has also been shown with this AAV1.cre construct [30,32]. Therefore, using this technique, reciprocally connected regions may include cells that are both transsynaptically anterogradely labeled and, to a lesser extent, retrogradely labeled. Previous studies have shown that the transsynaptic transport of the virus is monosynaptic, i.e. it does not cross additional synapses [24,30,31].

Injections were made in M1/M2 and performed as previously described [24]. Briefly, animals were anesthetized with isoflurane (4%; Baxter, Germany), the skull exposed and a small hole was drilled into the skull. We performed the cortical injection according to stereotaxic coordinates for M1/M2 injections (1.7 mm rostral, 1 mm lateral and 1 mm deep) derived from the mouse brain atlas in reference to bregma [33]. The injections were made via nanoliter delivery system (World Precision Instruments, Germany) and fine glass micropipettes (tip diameter 20 μm). A volume of 60 nl in 6 × 10 steps of the AAV1.cre construct (titer 3.0×10^{13} GC/mL) was injected over 10 min. After injections, craniotomies were sealed with bone wax (Ethicon, Johnson and Johnson, Germany) and the skin was closed with tissue adhesive (Histoacryl; B/Braun, Germany). Subsequently, the animals were returned to their home cages for 2 weeks to allow for protein expression.

2.3. Two-photon calcium imaging

Two-photon calcium imaging was performed using an 8 kHz resonant scanning microscope (HyperScope, Scientifica) with an Ultrafast laser (InSight X3 Dual output laser; Spectra-Physics; < 120 fs pulse width, 80 MHz repetition rate) tuned to 940 nm. Images were acquired at 30 Hz (using a 16X objective 0.8 NA, Nikon; tilted 30° from vertical for AuD imaging and 70° from vertical for A1 imaging) with ScanImage software (Vidrio Technologies). Imaging of layer 2/3 auditory cortex (at cortical depths between 160–280 μm) was performed in daily sessions across several days. For all imaging sessions, mice were awake, head restrained, and placed on an air-suspended polystyrene 20 cm ball. Each animal was habituated to the experimental set-up during the first 15 min before the experimental protocol was initiated and no significant differences in responses to locomotion were found across days; therefore, results are reported across sessions. Animals were in the dark for all

trials. Movements were monitored using a Jet Ball system (PhenoSys GmbH, sampling frequency 30 Hz). The sampling frequency of the optical encoders were resampled to precisely match the sampling frequency of the imaging. Loudspeakers (Genelec, Finland) were placed on both the right and left of the animal.

2.4. Auditory stimulation

Auditory stimuli were generated using inbuilt MATLAB functions (MathWorks, MA, USA) and consisted of temporally-repeated and superimposed frequency modulated (FM) sweeps that included 6 s ascending and 6 s descending repeated FM sweeps (at an interval of 83 ms) ranging between 8−20 kHz (at a speed of 12 kHz/s; 66 dB) to create an auditory illusion consisting of continuously ascending or descending pitches occurring at 1 Hz frequency (Fig. 1C; see also [34]). In each session, 70 trials (7 trials within 10 blocks of 90 s each) were presented. One trial (12 s long) consisted of frequency modulated sweeps of 6 s ascending and 6 s descending. Responses under ambient conditions were assessed by randomly interleaving 90 s blocks where no auditory stimulus was presented (10 blocks, 90 s each). The 'ambient' condition consists of the baseline noise in the room plus the additional noise of the resonance scanner (8 kHz; total 50 dB), which was present under all conditions. The start trigger for the presentation of the auditory stimuli was recorded using PhenoSys software (PhenoSys GmbH, sampling frequency 30 Hz) and, together with the movement encoder, aligned to the calcium imaging post hoc, where the stimulus trigger was matched to the imaging datafile by down-sampling and interpolating such that the aligned datasets had the same number of frames within each 90 s block.

2.5. Histology

Animals were deeply anesthetized with ketamine (20 mg/100 g body weight, ip) and xylazine (1 mg/100 g body weight, ip) and perfused transcardially with 20 mL of 0.1 M phosphate-buffered saline (PBS, pH 7.4) followed by 200 mL of 4% paraformaldehyde. To mark the location of the imaging site in the GCaMP6 transgenic mice, the cranial window was removed after perfusion and a pipette coated in red fluorescent latex microspheres (RetroBeads, Lumafluor Inc.) was inserted into the cortex (up to 1 mm deep) at the recording site, as indicated by a reference picture taken after the first imaging session (e.g. see Fig. 1E). In the PV.cre and wildtype mice, the AAV injection site also served to mark the location of the imaging site (for e.g. see Fig. 4B,C). The brains were then extracted, post-fixed overnight in 4% paraformaldehyde at 4 °C, and then cryoprotected in 30 % sucrose in PBS for 48 h.

Brains were cut into 40 µm thick coronal sections (CryoStar NX70, Thermo Scientific, USA) and collected in PBS (free-floating). For immunohistochemical staining, serial series of floating sections were then blocked in normal donkey serum (10 % and 0.4 % triton in PBS) for 1 h and incubated in primary antibodies overnight at 4 °C to visualize either parvalbumin (PV; monoclonal mouse anti-parvalbumin, 1:4000, Swant, PV 235; RRID: AB_10000343) or non-phosphorylated neurofilaments, (NNF; monoclonal mouse anti-Neurofilament H [NF-H], Nonphosphorylated, 1:2500, Biolegend 801701; RRID: AB_2564642). After rinsing in PBS, sections were incubated for 2 h with donkey anti-mouse Cy3 (Jackson ImmunoResearch Labs Cat# 715-165-150, RRID: AB_2340813, United Kingdom). Finally, sections were rinsed again in PBS, mounted on gelatin-coated slides, and coverslipped with MOWIOL (Fluka, Germany).

High resolution images were captured using a confocal microscope (Zeiss LSM 700, Germany) under a 2.5x objective (NA 0.085, Zeiss, Germany) and merged (resulting in ~4000 × 3000 pixel image per coronal section) using inbuilt functions for feature based panoramic image stitching in MatLab (Mathworks, MA, USA). Sections containing either the fluorescent bead track or the center of the viral expression site were visually identified and mapped on to the corresponding anterior-posterior image from the [33] mouse brain atlas according to the locations of the midbrain nuclei (Fig. 1F,H). PV staining further confirmed the location of AuD and A1 according to the atlas (see Fig. 1G; see also [19]). The NNF staining was then used to determine the approximate location of the imaging sites with regard to an auditory cortex functional atlas (as described in [21]; see Fig. 1G,H).

2.6. Data analysis

2.6.1. Image analysis

Images collected during two-photon calcium imaging were analyzed as previously described [9,35]. Briefly, images were motion corrected using discrete Fourier 2D-based image alignment of image frames (SIMA 1.3.2, sequential image analysis [36]). Regions of interest (ROIs) were demarcated manually and corresponded to all visually identifiable neuronal cell bodies in images downsampled to 1 Hz. During ROI segmentation experimenters are given generic animal IDs and blind to experimental timepoints within the data (i.e. stimulus onsets, behavioral state, etc.). The pixel intensity was then averaged within each ROI to create a raw fluorescence time series F(t). Baseline fluorescence F_0 was computed for each neuron by taking the 5th percentile of the smoothed F(t) (1 Hz lowpass, zero-phase, 60th-order FIR filter) and the change in fluorescence relative to baseline ($\Delta F/F_0$) was calculated ($F(t)-F_0/F_0$). We used nonnegative matrix factorization (NMF), in order to remove neuropil contamination as implemented in FISSA [37]. All further analyses were performed using custom-written scripts in MATLAB (MathWorks, MA, USA), which are freely available via GitHub (github.com/pakanlab/Henschke_et_al_CellCalcium2021).

2.6.2. Locomotion

The separation of locomotion and stationary periods from the movement encoder were calculated as previously described [9]. Briefly, stationary periods corresponded to frames where the instantaneous speed (as measured at the 30 Hz sampling rate) was less than 0.1 cm/s. Locomotion frames were identified when the instantaneous speed was >0.1 cm/s, 0.25 Hz lowpass filtered speed was >0.1 cm/s, and the average speed over a 2 s window centered on the frame was >0.1 cm/s. Any frames within an inter-locomotion interval shorter than 500 ms were also labeled as locomotion. Stationary periods less than 3 s after or 0.2 s before a period of locomotion were removed from the analysis (based on GCaMP6 kinetics [38]).

2.6.3. Sensory-evoked and locomotion modulation

To calculate the sensory-evoked modulation index (sensory-evoked MI), we first separated the data associated with one behavioral activity (locomotion or stationary), which was then averaged across each trial. The sensory-evoked MI was defined as the difference between the mean $\Delta F/F_0$ across all trials (for either stationary or locomotion periods) during the presentation of frequency modulated sweeps (R_F) and ambient (R_A) conditions, normalized by the sum:

$$\text{sensory-evoked MI} = (R_F - R_A)/(R_F + R_A).$$

The locomotion modulation index (locomotion MI) was calculated during blocks when the auditory stimulus was presented, and was defined as the difference between the mean $\Delta F/F_0$ during all locomotion (R_L) and stationary (R_S) periods, normalized by the sum:

$$\text{locomotion MI} = (R_L - R_S)/(R_L + R_S).$$

To determine the significant populations for the modulation indices we used bootstrapping to estimate the error on the locomotion MI and the sensory-evoked MI for each neuron (see also [9]). For the sensory-evoked MI, trials were separated into 6 s bins for both ambient and sensory evoked conditions, and the mean $\Delta F/F_0$ associated with one behavioral activity (locomotion or stationary) was averaged across each bin. For the locomotion MI, 1 s bins were taken along all data, each of

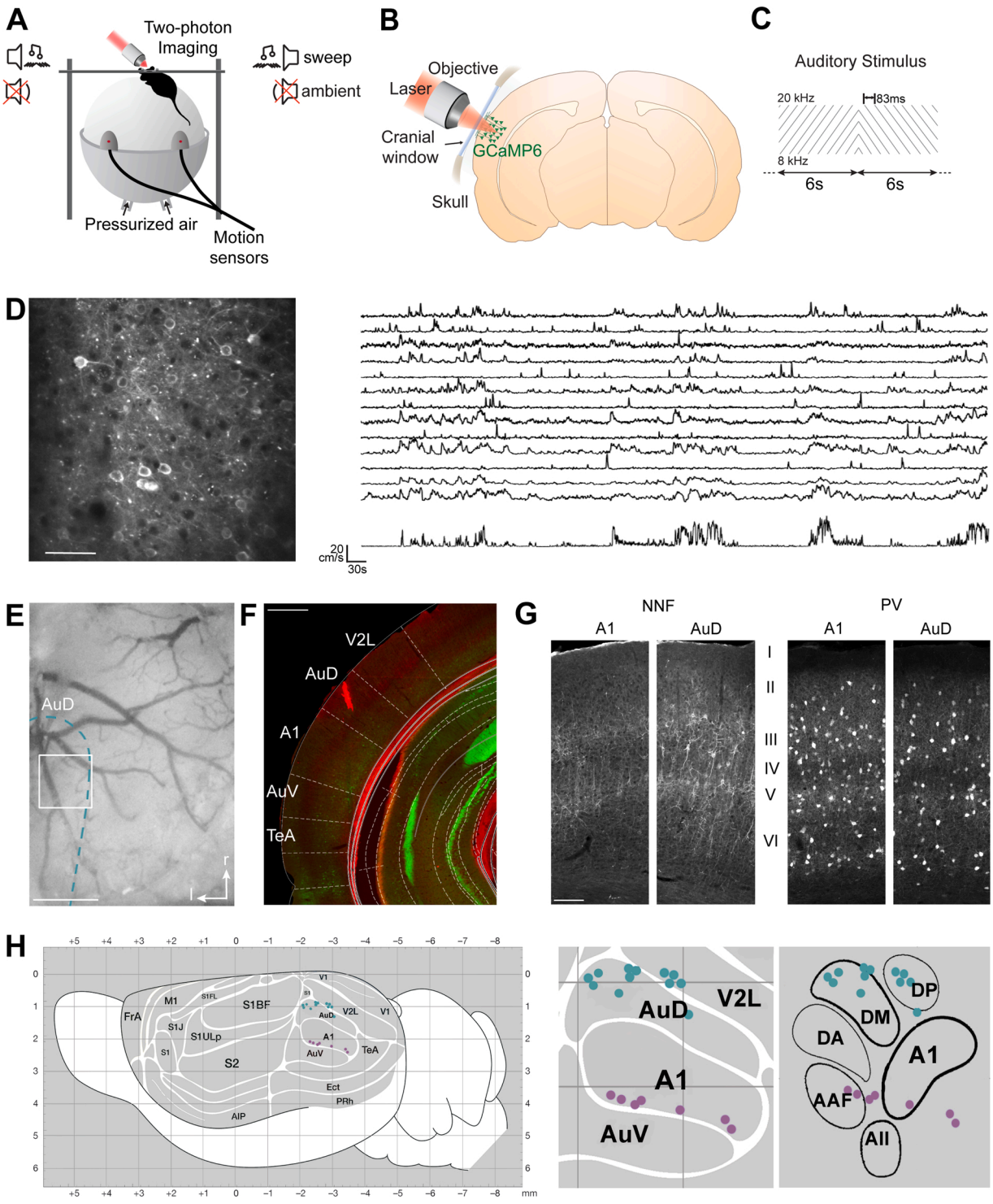

Fig. 1. Two-photon calcium imaging in auditory cortex and anatomical mapping of imaging sites. (A) Schematic of experimental set-up for two-photon calcium imaging of auditory cortex (B) in awake-behaving mice while head-fixed and able to run freely on a spherical treadmill during the presentation of a binaural auditory stimulus (C; frequency modulated sweep [sweep]) or during ambient conditions. (D) Two-photon imaging field-of- view with GCaMP6 labeled neurons (left) and change in fluorescence ($\Delta F/F_0$) for example neurons (right; normalized and set to an offset of one) aligned with the corresponding running speed (bottom). (E) Widefield image of cranial window demarcating the outline of a representative field-of-view in the dorsal auditory field(AuD). (F) Imaging site marked with retrobeads (red) and mapped to mouse atlas in coronal sections in GCaMP6f transgenic mice (green). (G) Neurofilament (NNF) and Parvalbumin (PV) immunostaining was used to further delineate primary auditory cortex (A1) and AuD. (H) Schematic of mouse brain (lateral-view) indicating imaging locations aligned to atlas coordinates (left, middle, based on [39]) or functional auditory map (right; based on [40]). Scale bars 50 μm (D), 500 μm (E,F), 100 μm (G).

which had one behavioral activity (locomotion or stationary) throughout its duration. For each bin, we took the mean $\Delta F/F_0$ and regarded this value as a single sample. For periods of time during which behavioral activity persisted for longer than 1 s, additional samples were drawn with intervals of no less than 2 s (based on the autocorrelation of the calcium fluorescence signal, which took approximately 2 s to fall to $R = 0.5$). For both modulation indices, randomly selected samples of $\Delta F/F_0$ with replacement were then selected from our original set of samples and this process was repeated 10,000 times to obtain 95 % confidence intervals for significance tests for each neuron individually. A neuron was considered significantly locomotion responsive or significantly responsive to the auditory stimulus if its 95 % confidence interval was significantly different from zero.

2.6.4. Statistics

In all graphs, the error bars indicate the standard error of the mean (s.e.m). Statistical tests used are indicated in the results. Either parametric or non-parametric statistics were used based on Lilliefors test of normality. For evaluation of responses on the population level, statistics were calculated across sessions, using each field-of-view as an independent sample. For evaluation of the distribution of individual neuronal responses or responses of selected neuronal subpopulations statistics were calculated across neurons.

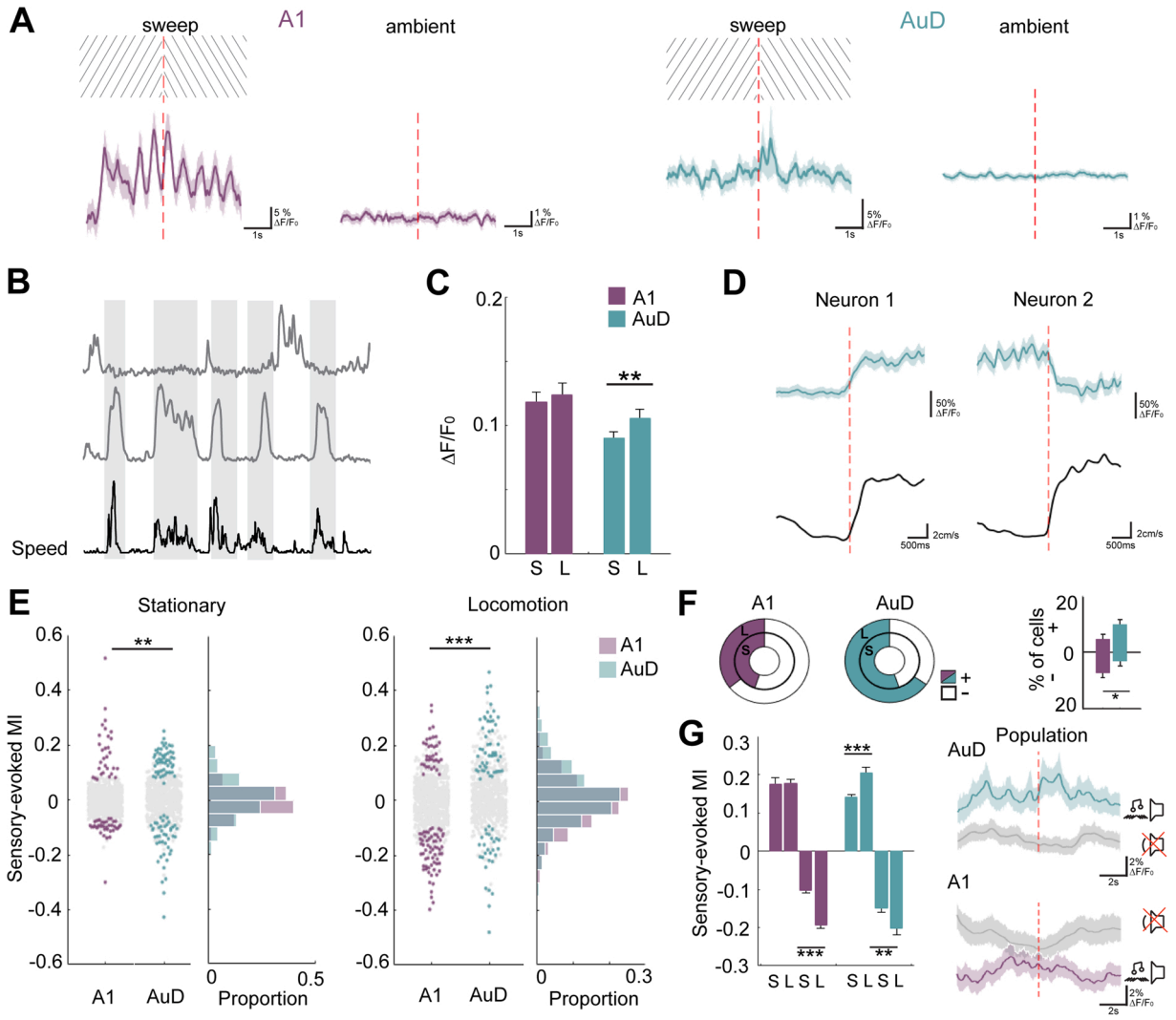

Fig. 2. Sensory-evoked responses are suppressed in the primary auditory cortex (A1) and more enhanced in dorsal auditory fields (AuD). (A) Mean change in fluorescence ($\Delta F/F_0$) across trials for an example neuron in A1 (left) and AuD (right), during presentation of an auditory stimulus (sweep) or ambient conditions. (B) Responses for two example neurons (grey) aligned with the corresponding running speed (black); grey shading indicates locomotion periods. (C) Mean $\Delta F/F_0$ during the presentation of the auditory stimulus averaged across imaging sessions for stationary (S) versus locomotion (L) periods. (D) Mean $\Delta F/F_0$ across locomotion periods aligned to locomotion onset (dashed line) for two example neurons in AuD (top); mean running speed is shown in black (bottom). (E) Distribution of sensory-evoked modulation index (MI) for all imaged neurons in A1 and AuD during stationary (left) and locomotion (right) periods. Significantly modulated neurons are indicated by coloured dots (determined by bootstrapping with resampling; 95 % confidence interval significantly different from zero). (F) Proportion of significantly modulated neurons with enhanced (+) or suppressed (-) sensory-evoked MI during stationary (S; inner ring) versus locomotion (L; outer ring) for A1 and AuD (left). Percentage of all neurons across sessions with significantly enhanced (+) or suppressed (-) sensory-evoked MI (right). (G) Average sensory-evoked MI for significantly modulated populations during stationary (S) and locomotion (L) periods (left). Example population responses during trials; $\Delta F/F_0$ during locomotion averaged across significantly modulated populations (AuD, enhanced populations; A1, suppressed populations) during the presentation of the auditory stimulus versus ambient conditions (as indicated by speaker symbol). * $p < 0.05$, ** $p < 0.01$, *** $p < 0.001$.

3. Results

3.1. Two-photon calcium imaging in mouse primary and dorsal auditory fields

We characterized the responses of layer $^2/_3$ neurons of the auditory cortex in head-fixed mice which were able to freely move on a spherical treadmill (Fig. 1A,B) during interleaved trials consisting of ambient noise or frequency modulated sweeps (ascending and descending sweeps of 8−20 kHz; Fig. 1C). To examine the responses of excitatory populations in the auditory cortex we first utilized transgenic mice expressing a genetically encoded calcium indicator, GCaMP6f [38], driven by a thy1 promoter (C57BL/6 J-Tg(Thy1-GCaMP6f) GP5.5Dkim/J). The mean change in fluorescence ($\Delta F/F_0$) for individual neurons was extracted for each field-of-view and synchronized with the running speed of the animal (Fig. 1D).

Within the auditory cortex, cranial windows were made over either the primary or the dorsal auditory field, using stereotaxic coordinates according to Paxinos and Franklin, 2008. Imaging locations were marked post-hoc by identifying the pattern of blood vessels within the cranial window during imaging (Fig. 1E) and marking the site with a glass pipette coated with retrograde beads (RetroBeads, Lumafluor Inc.; Fig. 1F). Coronal sections were then aligned to the atlas (Fig. 1F, [33]) and the boundaries of A1 and AuD were identified in combination with the expression pattern of NNF and PV (Fig. 1G; [19,21,33]). In this way, the location of the imaging sites were mapped and are shown overlaid on the auditory cortex borders according to the stereotaxic atlas [33] as well as a functionally defined auditory cortex map in mice for reference ([40]; Fig. 1H).

3.2. Modulation of sensory-evoked responses during stationary and locomotion periods

Individual excitatory neurons in both A1 and AuD demonstrated stimulus-evoked responses to the frequency modulated sweeps (Fig. 2A), with AuD neurons more selective to either up/down sweeps or transitions (see also [34,41]). We examined how the auditory responses of neurons in A1 and AuD were altered during changes in behavioral state by separating out locomotion periods when the animals were running on the spherical treadmill and stationary periods when animals were quiescent (e.g. Fig. 2B). On the population level, we found no significant difference between the mean response during stationary versus locomotion periods in A1 across sessions ($\Delta F/F_0$: stationary 0.12 ± 0.01, locomotion 0.12 ± 0.01; $p = 0.805$; $n = 7$; paired t test); however, the mean response during locomotion was significantly higher than that of stationary periods in AuD (Fig. 2C; $\Delta F/F_0$: stationary 0.09 ± 0.01, locomotion 0.11 ± 0.01; $p = 0.002$; $n = 12$; paired t test). On the single-cell level, in A1 as well as in AuD we observed heterogeneous responses to locomotion periods, with excitatory neurons demonstrating both increased as well as decreased activity aligned to the onset of locomotion (Fig. 2D).

To quantify the effects of changes in behavioral state on the sensory-evoked responses in the auditory cortex, we first isolated stationary and locomotion periods and then calculated a sensory-evoked modulation index (sensory-evoked MI) for each. This corresponds to the difference between the mean $\Delta F/F_0$ during the presentation of frequency modulated sweeps (R_F) and during ambient (R_A) conditions, normalized by the sum of the mean $\Delta F/F_0$ for both conditions (sensory-evoked MI = $(R_F - R_A)/(R_F + R_A)$). We found a significant difference in the distribution of sensory-evoked responses between A1 and AuD during stationary and locomotion periods (Fig. 2E; stationary: $p = 0.001$; locomotion: $p < 0.001$; Kruskal-Wallis test). Specifically, we found that the sensory-evoked responses were significantly enhanced by locomotion in a larger proportion of AuD neurons (53/653) in comparison to A1 (35/780), while responses were significantly suppressed by locomotion in more A1 neurons (63/780) in comparison to AuD (28/653; Fig. 2F). This was also reflected on the population-level across sessions (suppressed: A1 $8 \pm 2\%$, AuD $3 \pm 2\%$; $p = 0.037$; enhanced: A1 $5 \pm 2\%$, AuD $10 \pm 2\%$; $p = 0.058$; Mann–Whitney U test). Similarly, the magnitude of the sensory-evoked modulation for the population of neurons enhanced by locomotion was significantly greater in AuD (mean sensory-evoked MI: stationary 0.14 ± 0.01, locomotion 0.20 ± 0.01; $p < 0.001$; Mann–Whitney U test), but remained unchanged in A1 (mean sensory-evoked MI: stationary 0.18 ± 0.02, locomotion 0.18 ± 0.01; $p = 0.961$; Mann–Whitney U test), and suppressed populations in both regions showed a stronger magnitude of suppression during locomotion (Fig. 2G; A1: stationary -0.10 ± 0.01, locomotion -0.19 ± 0.01; $p < 0.001$; AuD: stationary -0.15 ± 0.01, locomotion -0.20 ± 0.02; $p < 0.001$; Mann–Whitney U test). Altogether, our findings suggest that, compared to A1, the activity of excitatory neurons in AuD is generally more enhanced by movement.

3.3. Connections from motor cortex to PV and non-PV populations in the auditory cortex

Previous studies have established the existence of direct projections from motor cortex to generalized regions in the auditory cortex [12,26,27,42] and suggested this cortico-cortical pathway is directly involved in flexible movement-related suppression [12,14,16,43]. Additionally, it has been shown that PV interneurons in the auditory cortex can, at least in part, mediate movement-evoked changes in activity via direct projections from motor cortex [12,13,42]. Given our finding that the responses of excitatory neurons in AuD are generally more enhanced during locomotion, we next investigated the underlying cell-type specific circuitry between projections from the motor cortex to both primary and dorsal regions of the auditory cortex. To do this we injected a mono-transsynaptic anterograde virus, AAV1.cre (Fig. 3A,B; [24,30,31]), into the motor cortex (M1/M2 regions; Fig. 3B) and examined the resulting labelling within the auditory cortex (Fig. 3C). We found a larger proportion of labeled cells within AuD compared to A1 (Fig. 3C, D), indicating a greater proportion of cells in AuD are mono-synaptically connected to the motor cortex. We found that the majority of labeled cells were located in deep cortical layers, although this was not exclusively the case (e.g. see Fig. 3C). Note that since the AAV1.cre virus travels mono-trans-synaptically, largely in the anterograde direction, but has a low efficiency for retrograde transfection at the injection site [30], some labeled cells in the auditory cortex may represent projections from the auditory cortex to the motor cortex, since these regions are reciprocally connected [26,27,44]. Regardless, we also found denser terminal labelling in AuD, largely located in cortical layer 6 and to lesser extent layer 1 (see Fig. 3F; see also [27], again confirming denser anterograde projections from motor cortex.

To examine the proportion of PV interneurons receiving direct connections from the motor cortex, we additionally used immunohistochemistry to visualize PV-expression. We confirmed that A1 has a larger proportion of PV-expressing cells (Fig. 3E; see also [19]), however when we examined the relative proportion of PV-expressing neurons that also receive direct projections from the motor cortex, we found that a similar proportion of cells were double labeled in both regions, 7% and 9% in A1 and AuD, respectively (Fig. 3F,G), which is also representative of the general proportion of PV-expressing interneurons within the cerebral cortex [45,46]. We also found that the majority of double-labeled PV interneurons were located in deep cortical layers (e.g. Fig. 3F). Note that since cortical PV cell axons make largely local connections and do not generally send long-range cortico-cortical projections [47,48], the observed double labeled PV populations are likely a result of anterograde transsynaptic labelling from motor cortex regions and not retrograde labelling. Therefore, AuD showed more general connectivity to the motor cortex but the relative proportion of motor cortex projections specifically to PV interneurons versus non-PV neurons was similar to that of A1.

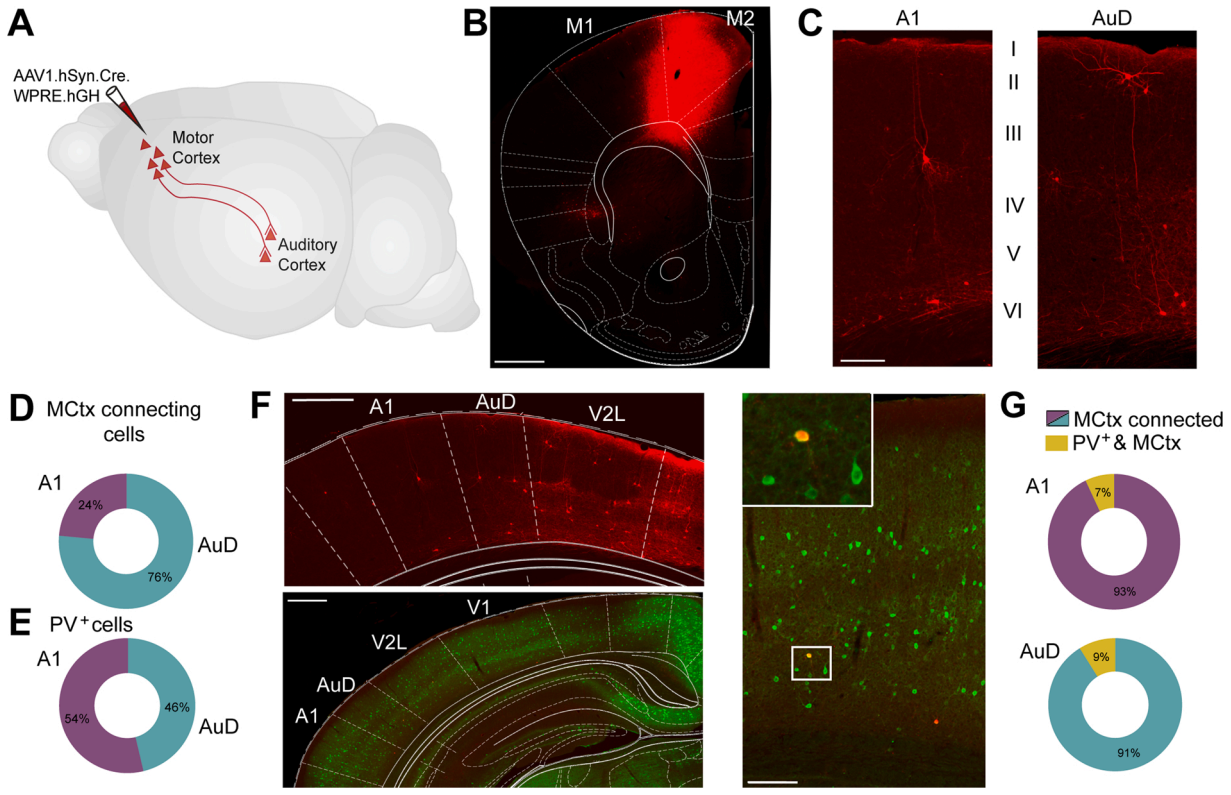

Fig. 3. Transsynaptic tracing of projections from motor cortex to primary (A1) and dorsal (AuD) auditory cortex in parvalbumin (PV) expressing and non-PV populations reveal AuD is more highly connected to motor cortex. (A) Schematic of mono-trans-synaptic anterograde tracing method (B) Image of coronal section showing representative injection site into motor cortex with overlaid stereotaxic atlas [33]. (C) Resulting labelling in A1 and AuD following injection in (B). (D) Percentage of the number of resulting neurons labeled in A1 and AuD following injections in the motor cortex. (E) Percentage of the total number of PV-expressing neurons normalized by area in A1 compared to AuD. (F) Images of coronal sections after injections of the AAV1.cre into the motor cortex (left, top) and the distribution of PV-expressing neurons in the auditory cortex (left, bottom). Double labeled neuron following AAV1.cre injection in motor cortex and PV immunostaining in AuD. (G) Percentage of labeled neurons in A1 and AuD following AAV1.cre injections in motor cortex that are also PV-expressing. Scale bars 500 μm (B, F left), 100 μm (C, F right).

3.4. Locomotion-evoked cell-type specific response modulation in AuD

To determine the motor-evoked cell-type specific responses of the PV-expressing interneuron population within AuD, we then injected a cre-dependent AAV to drive the expression of GCaMP6m in PV.cre transgenic mice (B6;129P2-Pvalb$^{tm1(cre)Arbr}$/J; Fig. 4A,B) and imaged the responses of PV-expressing interneurons (272 cells across 10 sessions) during stationary and locomotion periods in the presence of the auditory stimulus. Additionally, to obtain comparative data from all neuronal cell types in AuD (i.e. both excitatory and all inhibitory populations), we also injected an AAV which drives the expression of GCaMP6m in wildtype mice (C57BL/6 J mice; Fig. 4C; 730 cells across 11 sessions). Interestingly, we found no significant difference in the mean population activity between stationary and locomotion periods for the PV population ($\Delta F/F_0$: stationary 0.19 ± 0.01, locomotion 0.17 ± 0.01; $p = 0.255$; $n = 10$; paired *t* test), but the mean response of the population of all cells, labeled in wildtype mice, in AuD was significantly enhanced by locomotion (Fig. 4D; $\Delta F/F_0$: stationary 0.11 ± 0.01, locomotion 0.15 ± 0.01; $p = 0.005$; $n = 11$; paired *t* test), similar to the population of excitatory neurons in AuD (see Fig. 2C). However, on the single-cell level, we again found that individual PV neurons showed both enhanced or suppressed responses following locomotion onset (Fig. 4E). This modulation was clearly linked to locomotion onset, as was evident when we examined the average responses across all PV neurons that were significantly enhanced or suppressed by locomotion (Fig. 4F,G).

To quantify the direct influence of locomotion on neuronal responses in AuD, we calculated a locomotion MI as the difference between the mean $\Delta F/F_0$ during locomotion (R_L) and stationary (R_S) periods, normalized by the sum of the mean $\Delta F/F_0$ for both conditions (locomotion MI = $(R_L - R_S)/(R_L + R_S)$). We compared the locomotion MI across populations of PV interneurons, excitatory neurons, and the separate population of all neurons and found a significant difference in the distribution of locomotion modulated responses between the three populations (Fig. 4G; all comparisons $p < 0.001$; Kruskal-Wallis test with Bonferroni correction for multiple comparisons). Specifically, we found that a larger proportion of PV interneurons were suppressed by locomotion (121/272) in comparison to the excitatory population (27/653) or the general population of all neurons (56/730), and a larger proportion of the populations of all neurons were enhanced by locomotion (297/730) in comparison to either the excitatory population (111/653) or PV interneurons (34/272). This was also reflected on the population-level across sessions (Fig. 4H; PV: $p < 0.001$; Exc: $p = 0.002$; All: $p = 0.007$; Mann–Whitney *U* test). For all three populations, the sensory-evoked MI during locomotion was greater for the proportion of cells that were enhanced by locomotion compared to those that were suppressed (Fig. 4I; PV: $p = 0.027$; Exc: $p < 0.001$; All: $p < 0.001$; Mann–Whitney *U* test); i.e., neurons that increased their activity during locomotion were also more responsive to the presented auditory stimulus.

Since the proportion of excitatory to PV-expressing neurons is ~8:1 in the cerebral cortex [46], we calculated a weighted proportion of modulated cells from the PV and excitatory data to compare to the population of all cells. The results indicate that the PV and excitatory populations together may account for the population of suppressed responses observed in the population of all cells during locomotion, since there was no significant difference between this and the weighted population (All: $9 \pm 3\%$, weighted: $9 \pm 2\%$; $p = 0.161$; Mann–Whitney *U*

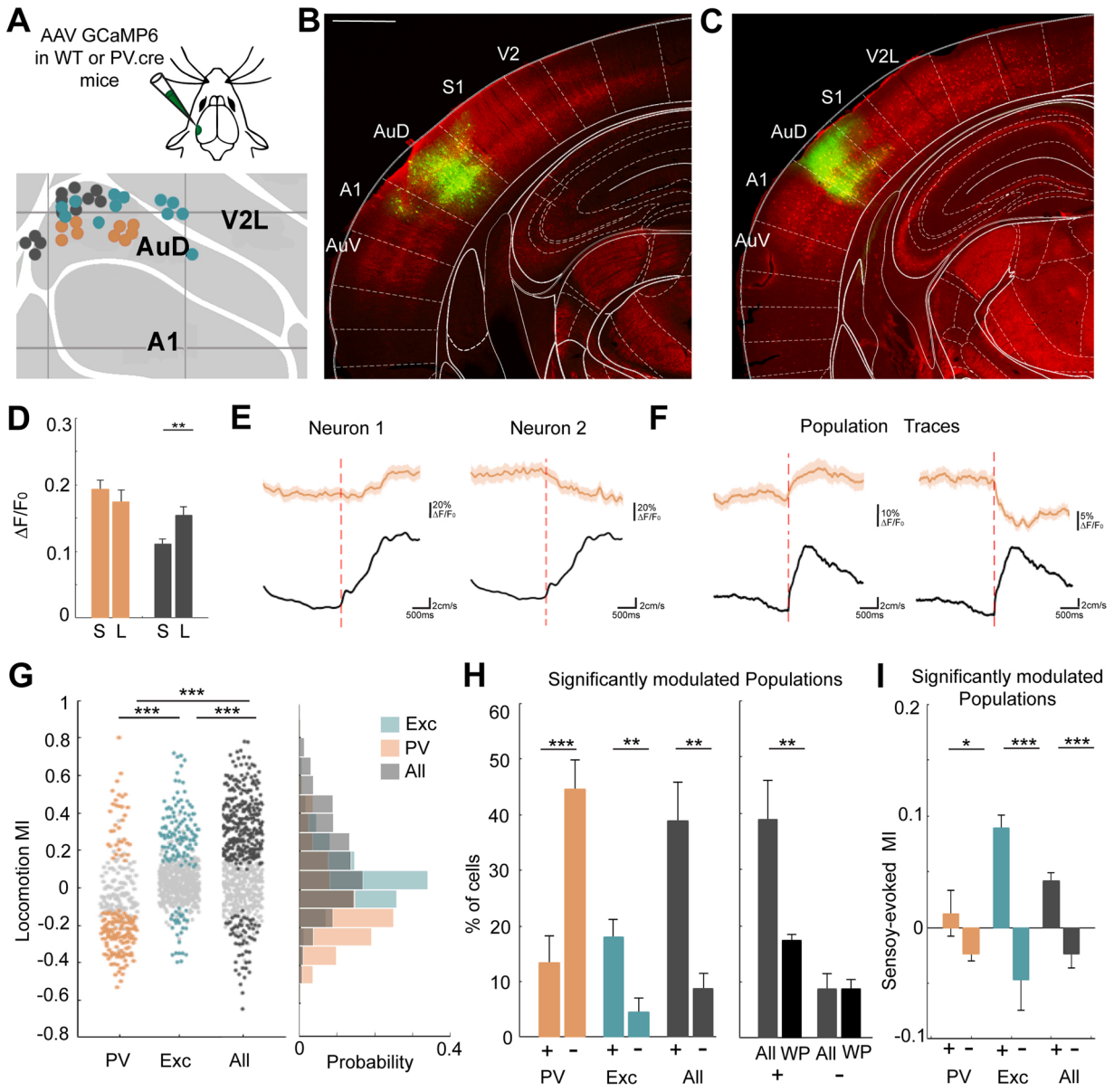

Fig. 4. Parvalbumin (PV) interneurons are largely suppressed and excitatory neurons enhanced by locomotion in dorsal auditory fields (AuD). (A) Schematic of lateral brain surface indicating imaging locations aligned to atlas coordinates (based on [39]) in PV.cre mice (PV-expressing interneurons; orange), GCaMP6 mice (excitatory cells [Exc]; teal), and wildtype mice (resulting in a population of all neuronal cell types being labeled [All]; grey). (B) Example injection site of cre-dependent AAV to drive expression of GCaMP6 (green) in AuD and neurofilament immunostaining (NNF; red) in PV.cre transgenic mice, with overlaid stereotaxic atlas [33]. (C) Example injection site of AAV to drive expression of GCaMP6 (green) in AuD and PV immunostaining (red) in wildtype mice, with overlaid stereotaxic atlas [33]. (D) Mean $\Delta F/F_0$ during the presentation of the auditory stimulus averaged across imaging sessions for stationary (S) versus locomotion (L) periods in the population of imaged PV interneurons (orange) and the population of all cell types in wildtype mice (grey) imaged in AuD. (E) Mean $\Delta F/F_0$ across locomotion periods aligned to locomotion onset (dashed line) for two example PV neurons in AuD with associated mean running speed (black). (F) Mean $\Delta F/F_0$ across locomotion periods aligned to locomotion onset (dashed line) for the population of PV neurons significantly modulated by locomotion in AuD with associated mean running speed (black). (G) Distribution of locomotion modulation index (MI) for populations of neurons in AuD. Significantly modulated neurons are indicated by colored dots (determined by bootstrapping with resampling; 95 % confidence interval significantly different from zero). (H) Percentage of significantly modulated neurons across sessions with enhanced (+) or suppressed (-) locomotion MI during stimulus presentation for each population (left). Comparison of the population of all cell types in wildtype mice with a weighted population (WP) of Exc and PV cells combined (8:1 ratio). (I) Average sensory-evoked MI for significantly modulated populations from (G) with enhanced (+) or suppressed (-) locomotion MI during stimulus presentation. Scale bars on image 500 μm (B). * $p < 0.05$, ** $p < 0.01$, *** $p < 0.001$.

test). However, using this method, there remained a residual proportion of neurons with significantly enhanced responses to locomotion in the population of all cells in comparison to the weighted population (All: $39 \pm 7\%$, weighted: $17 \pm 1\%$; $p = 0.001$; Mann–Whitney *U* test; Fig. 4H). Therefore, the majority of PV interneurons in AuD were suppressed during locomotion periods and the population representing all neuronal cell types had a disproportionately large number of cells with enhanced activity during locomotion, which was not reflected in the excitatory neuron or PV interneuron populations within AuD.

4. Discussion

4.1. Locomotion-evoked modulation of responses in primary versus dorsal auditory fields

Sensory processing in the cerebral cortex is highly modulated by changes in behavioral state and active behaviors [3,5,6,17,49,50]. Advancements in our understanding of how motor behaviors directly influence sensory systems have recently been hastened by experimental investigations in awake behaving animals; particularly with our ability to directly visualize area-specific and cell-type specific populations of neurons in awake head-fixed animals using two-photon calcium imaging [5,28,51,52]. Using these techniques, in the current study we have revealed functional differences in the modulation of sensory-evoked responses during locomotion between primary and dorsal auditory fields. Our results indicate that responses of layer $^{2}/_{3}$ excitatory neuron populations in AuD are generally more enhanced during locomotion, while those in A1 are more suppressed. Movement-evoked suppression of auditory responses has been previously demonstrated in mouse auditory cortex [12,13,15–17], and has been proposed to function as a cortical filter, with corollary discharge signals suppressing self-generated sounds while maintaining sensitivity to relevant environmental stimuli [12,43,53]. Similarly, this motor-evoked auditory suppression has also been described in human auditory cortex [54–56]. Interestingly, a study in humans using electrocorticographic activity from neurosurgical subjects found that the auditory cortex did not show uniform suppression during self-generated movements during speech, but that it was functionally suppressed in a specific topographical pattern [57]. In general, movement-related suppression in mice has been attributed to A1 cortical regions, although the precise mapping of cortical location within the auditory cortex is not always specified (although, see [16]). In contrast, excitatory populations in the visual and somatosensory cortex in mice, both of which are directly adjacent to dorsal auditory regions, have been shown to exhibit largely enhanced sensory-evoked responses during locomotion [7–11,58–60]. It is possible that there is a spatially organized gradient of locomotion-evoked responses from enhancement to suppression in the transition from visual/somatosensory to auditory cortices; indeed, here we confirm that the organization of projections from motor cortex would support this, with AuD being more highly connected to motor cortical regions in comparison to A1.

Functional differences between primary and dorsal auditory regions have also been previously reported in relation to stimulus-specific auditory processing. For instance, dorsoposterior and secondary auditory fields have been shown to be non-tonotopically organized with more specialized response properties [18,41,61,62]. In this study we presented frequency modulated sweeps, which have been shown to elicit responses in dorsal auditory fields [34] however, is not an optimal stimulus for tonotopic investigations. This may explain the modest proportion of excitatory neurons that showed strong stimulus-evoked responses (although auditory cortex in awake mice has also been shown to have a sparse representation of sound [63]), however, the comparative magnitude of these responses between stationary and locomotion periods remain clear — with more sensory-evoked suppression in A1 and more enhanced modulation in AuD. The functional differences between these two regions would suggest that while primary, tonotopically organized, auditory regions may contribute more to cortical filtering of relevant auditory stimuli [43], dorsal auditory fields may be more related to auditory spatial localization or similar tasks where enhanced movement-dependent sensory processing would be beneficial. There is some supporting evidence that this may be the case in larger mammals such as in cats [64,65] as well as monkeys, where neurons in caudal belt areas of auditory cortex, an early auditory dorsal stream region, have been shown to have higher spatial selectivity than those in A1 [66–68]. Similar functional distinctions in posterior auditory regions have also been described in humans [69]. While studies extending beyond A1 have not been extensive in mice, it has been shown that dorsal auditory fields respond to more complex stimuli [70] and have functional properties attributed to 'higher-order' auditory regions [62]. Additionally, AuD has a direct cortico-ponto-cerebellar pathway in mice that is not observed in A1 [24], which is interesting considering the role of the cerebellum in motor functions [71], but also in predictive sensory processing including sound localization [72–75]. Finally, while the auditory simulation in our experiments was not task-dependent or behaviorally-relevant, previous studies have shown that motor-related suppression demonstrates plasticity with learning and task-engagement [16,43,76]. Layer 6 corticothalamic neurons in the auditory cortex showed increased activity in response to orofacial movements linked to reward, but not task-irrelevant locomotion [77] (although see also [78]). Hence, interesting future studies could investigate dynamics related to experience-dependent plasticity that may differ across primary and dorsal auditory regions.

4.2. Cell-type specific response modulation in AuD

Cell-type specific functional circuitry, specifically, interactions between excitatory pyramidal cells and local interneuron populations, is known to be a vital component underlying the behavioral-state modulation of sensory processing [5,79,80]. Mechanisms of both feedforward inhibition [12,13] and balanced inhibition/excitation [14,16] via PV interneurons have been demonstrated in A1 in response to movement. In the current study, we investigated populations of excitatory neurons, PV interneurons, and the general population of all neurons in AuD. Perhaps unsurprisingly, we found that all populations showed heterogeneous responses [81] to locomotion-onset in AuD, however there were clear net effects across populations; with PV neurons showing largely suppression, and excitatory neurons as well as the general population of AuD neurons showing largely enhanced responses during locomotion periods. Interestingly, we found that the subpopulation of PV cells that significantly enhanced their responses during locomotion were also more responsive to the presented auditory stimulus. This is in agreement with results from a previous study in the auditory cortex demonstrating that after a reafferent stimulus was paired with locomotion, stimulus-selective inhibitory neurons received enhanced motor cortical input and increased their activity during locomotion, resulting in selective sound-evoked suppression in excitatory cells [43]. In the current study, we observed that the same ratio of PV-expressing to non-PV neurons received motor cortical input in both A1 and AuD; therefore, it is likely that this population of locomotion-enhanced PV cells in AuD also contribute to the suppressive effects we see in a subpopulation of local excitatory cells. The difference being that while this is the dominant circuitry in A1 [12,13], in AuD we observed a much larger proportion of PV interneurons that are suppressed at locomotion-onset as well as excitatory neurons that show enhanced activity with locomotion.

The net enhanced activity during locomotion in AuD pyramidal neurons may occur through a combination of factors, namely, an increased excitatory drive to pyramidal cells directly from the motor cortex as well as a decreased inhibitory drive of PV cells onto excitatory neurons. With regard to the later, this is likely to occur through disinhibition, acting via PV interneurons and originating from a separate interneuron population. Our current results provide support for this; when we imaged the activity of all neurons in AuD, we observed a population of cells that showed highly enhanced activity during locomotion and were not represented within the PV-expressing or excitatory populations alone. Disinhibitory circuits via suppression of PV interneurons have been previously described in the auditory cortex, for instance, in relation to the activation of somatostatin (SST) interneurons [70]. Additionally, pyramidal neuron disinhibition has also been demonstrated after activation of vasointestinal peptide (VIP) expressing interneurons in auditory cortex [15]; however, this disinhibitory circuit is generally thought to act via suppression of SST interneurons, as VIP neurons have fewer projections directly to PV cells [82]. VIP

interneurons are also known to be highly responsive to arousal/locomotion in other sensory cortices [9,83–85] and abundant in layer $^{2}/_{3}$ [86,87]; therefore, it is possible that they make up a substantial proportion of our observed highly modulated population within AuD, although further studies are needed.

5. Conclusion

How local and long-range circuit dynamics in sensory cortices are influenced by changes in behavioral state are important questions to increase our understanding of how the brain integrates sensory and motor information. Although the mouse has not traditionally been a model organism for auditory investigations, the growing importance of this animal model in modern neuroscience, and the flexibility offered through the use of advanced imaging techniques as well as genetic tools and manipulations, means that an understanding of the structural and functional principles of the mouse auditory system is warranted. Interactions between motor and auditory systems have also proven to be conserved across many vertebrate species [17]. The functional divergence between primary and dorsal auditory fields that we have demonstrated in the current study, is an important step towards this understanding and may prove to be an important distinction for auditory processing during navigation and acoustically guided behavior.

CRediT authorship contribution statement

Julia U. Henschke: Conceptualization, Methodology, Validation, Formal analysis, Investigation, Data curation, Writing - original draft, Writing - review & editing, Visualization. **Alan T. Price:** Methodology, Investigation, Writing - review & editing, Visualization. **Janelle M.P. Pakan:** Conceptualization, Methodology, Formal analysis, Writing - original draft, Writing - review & editing, Supervision, Funding acquisition.

Declaration of Competing Interest

The authors have no conflicts of interest to report pertaining to this study.

Acknowledgements

We are grateful to Cathleen Knape for expert technical assistance. We thank the GENIE Program and the Janelia Research Campus, specifically V. Jayaraman, R. Kerr, D. Kim, L. Looger, and K. Svoboda, for making GCaMP6 available. This work was funded by the European Regional Development Fund (ERDF: Center for Behavioral Brain Sciences ZS/2016/04/78113) to JUH, ATP and JMPP, and by the Deutsche Forschungsgemeinschaft (DFG, German Research Foundation) – Project-ID 425899996 – SFB 1436 to JMPP.

References

[1] T.B. Crapse, M.A. Sommer, Corollary discharge across the animal kingdom, Nat. Rev. Neurosci. 9 (August (8)) (2008) 587–600.
[2] H. Straka, J. Simmers, B.P. Chagnaud, A new perspective on predictive motor signaling, Curr. Biol. 28 (March 5 (5)) (2018) R232–43.
[3] L. Busse, J. Cardin, M.E. Chiappe, M.M. Halassa, M.J. McGinley, T. Yamashita, et al., Sensation during active behaviors, J. Neurosci. (2017).
[4] A.G. Khan, S.B. Hofer, Contextual signals in visual cortex, Curr. Opin. Neurobiol. 52 (October) (2018) 131–138.
[5] J.M.P. Pakan, V. Francioni, N.L. Rochefort, Action and learning shape the activity of neuronal circuits in the visual cortex, Curr. Opin. Neurobiol. 52 (October) (2018) 88–97.
[6] D.M. Schneider, Reflections of action in sensory cortex, Curr. Opin. Neurobiol. 64 (October 1) (2020) 53–59.
[7] S. Erisken, A. Vaiceliunaite, O. Jurjut, M. Fiorini, S. Katzner, L. Busse, Effects of locomotion extend throughout the mouse early visual system, Curr. Biol. 24 (December 15 (24)) (2014) 2899–2907.
[8] C.M. Niell, M.P. Stryker, Modulation of visual responses by behavioral state in mouse visual cortex, Neuron. 65 (February 25 (4)) (2010) 472–479.
[9] J.M.P. Pakan, S.C. Lowe, E. Dylda, S.W. Keemink, S.P. Currie, C.A. Coutts, et al., Behavioral-state modulation of inhibition is context-dependent and cell type specific in mouse visual cortex, Mrsic-Flogel TD, editor, eLife 5 (August 23) (2016), e14985.
[10] A. Ayaz, A. Stäuble, M. Hamada, M.-A. Wulf, A.B. Saleem, F. Helmchen, Layer-specific integration of locomotion and sensory information in mouse barrel cortex, Nat. Commun. 10 (June 13 (1)) (2019) 2585.
[11] N.J. Sofroniew, Y.A. Vlasov, S.A. Hires, J. Freeman, K. Svoboda, Neural coding in barrel cortex during whisker-guided locomotion, Nelson SB, editor, eLife 4 (December 23) (2015), e12559.
[12] A. Nelson, D.M. Schneider, J. Takatoh, K. Sakurai, F. Wang, R. Mooney, A circuit for motor cortical modulation of auditory cortical activity, J Neurosci Off. J. Soc. Neurosci. 33 (September 4 (36)) (2013) 14342–14353.
[13] D.M. Schneider, A. Nelson, R. Mooney, A synaptic and circuit basis for corollary discharge in the auditory cortex, Nature 513 (September 11 (7517)) (2014) 189–194.
[14] M. Zhou, F. Liang, X.R. Xiong, L. Li, H. Li, Z. Xiao, et al., Scaling down of balanced excitation and inhibition by active behavioral states in auditory cortex, Nat. Neurosci. 17 (June (6)) (2014) 841–850.
[15] J. Bigelow, R.J. Morrill, J. Dekloe, A.R. Hasenstaub, Movement and VIP interneuron activation differentially modulate encoding in mouse auditory cortex, eNeuro 6 (September 1 (5)) (2019).
[16] B.P. Rummell, J.L. Klee, T. Sigurdsson, Attenuation of responses to self-generated sounds in auditory cortical neurons, J. Neurosci. Off. J. Soc. Neurosci. 36 (November 23 (47)) (2016) 12010–12026.
[17] D.M. Schneider, R. Mooney, How movement modulates hearing, Annu. Rev. Neurosci. 41 (1) (2018) 553–572.
[18] H. Tsukano, M. Horie, R. Hishida, K. Takahashi, H. Takebayashi, K. Shibuki, Quantitative map of multiple auditory cortical regions with a stereotaxic fine-scale atlas of the mouse brain, Sci. Rep. 6 (February 29) (2016) 22315.
[19] S.J. Cruikshank, H.P. Killackey, R. Metherate, Parvalbumin and calbindin are differentially distributed within primary and secondary subregions of the mouse auditory forebrain, Neuroscience 105 (3) (2001) 553–569.
[20] R. Gămănuţ, H. Kennedy, Z. Toroczkai, M. Ercsey-Ravasz, D.C. Van Essen, K. Knoblauch, et al., The mouse cortical connectome, characterized by an ultra-dense cortical graph, maintains specificity by distinct connectivity profiles, Neuron 97 (February 7 (3)) (2018) 698–715.e10.
[21] M. Horie, H. Tsukano, H. Takebayashi, K. Shibuki, Specific distribution of non-phosphorylated neurofilaments characterizing each subfield in the mouse auditory cortex, Neurosci. Lett. 606 (October 8) (2015) 182–187.
[22] E. Budinger, P. Heil, H. Scheich, Functional organization of auditory cortex in the Mongolian gerbil (Meriones unguiculatus). III. Anatomical subdivisions and corticocortical connections, Eur. J. Neurosci. 12 (July (7)) (2000) 2425–2451.
[23] H. Tsukano, M. Horie, K. Takahashi, R. Hishida, H. Takebayashi, K. Shibuki, Independent tonotopy and thalamocortical projection patterns in two adjacent parts of the classical primary auditory cortex in mice, Neurosci. Lett. 637 (January 10) (2017) 26–30.
[24] J.U. Henschke, J.M. Pakan, Disynaptic cerebrocerebellar pathways originating from multiple functionally distinct cortical areas, eLife. 9 (August 14) (2020).
[25] H. Tsukano, X. Hou, M. Horie, H. Kitaura, N. Nishio, R. Hishida, et al., Reciprocal connectivity between secondary auditory cortical field and amygdala in mice, Sci. Rep. 9 (December 23 (1)) (2019) 19610.
[26] S.W. Oh, J.A. Harris, L. Ng, B. Winslow, N. Cain, S. Mihalas, et al., A mesoscale connectome of the mouse brain, Nature 508 (April 10 (7495)) (2014) 207–214.
[27] B. Zingg, H. Hintiryan, L. Gou, M.Y. Song, M. Bay, M.S. Bienkowski, et al., Neural networks of the mouse neocortex, Cell 156 (February 27 (5)) (2014) 1096–1111.
[28] E. Dylda, J.M.P. Pakan, N.L. Rochefort, Chapter 13 - chronic Two-photon calcium imaging in the visual cortex of awake behaving mice, in: D. Manahan-Vaughan (Ed.), Handbook of Behavioral Neuroscience, Elsevier, 2018 [cited 2021 Jan 25]. p. 235–251. (Handbook of Neural Plasticity Techniques; vol. 28).
[29] F. Zhao, H.-F. Jiang, W.-B. Zeng, Y. Shu, M.-H. Luo, S. Duan, Anterograde trans-synaptic tagging mediated by adeno-associated virus, Neurosci. Bull. 33 (January 31 (3)) (2017) 348–350.
[30] B. Zingg, X.-L. Chou, Z.-G. Zhang, L. Mesik, F. Liang, H.W. Tao, et al., AAV-mediated anterograde transsynaptic tagging: mapping corticocollicular input-defined neural pathways for defense behaviors, Neuron 93 (January 4 (1)) (2017) 33–47.
[31] B. Zingg, B. Peng, J. Huang, H.W. Tao, L.I. Zhang, Synaptic specificity and application of anterograde transsynaptic AAV for probing neural circuitry, J. Neurosci. 40 (April 15 (16)) (2020) 3250–3267.
[32] D.G.R. Tervo, B.-Y. Hwang, S. Viswanathan, T. Gaj, M. Lavzin, K.D. Ritola, et al., A designer AAV variant permits efficient retrograde access to projection neurons, Neuron 92 (October 19 (2)) (2016) 372–382.
[33] G. Paxinos, Franklin, The mouse brain in stereotaxic coordinates. Compact: The Coronal Plates and Diagrams, Elsevier Science, 2008, p. 256.
[34] Y. Honma, H. Tsukano, M. Horie, S. Ohshima, M. Tohmi, Y. Kubota, et al., Auditory cortical areas activated by slow frequency-modulated sounds in mice, PLoS ONE 8 (July 17 (7)) (2013).
[35] J.M.P. Pakan, S.P. Currie, L. Fischer, N.L. Rochefort, The impact of visual cues, reward, and motor feedback on the representation of behaviorally relevant spatial locations in primary visual cortex, Cell Rep. 24 (September 4 (10)) (2018) 2521–2528.
[36] P. Kaifosh, J.D. Zaremba, N.B. Danielson, A. Losonczy, SIMA: python software for analysis of dynamic fluorescence imaging data, Front Neuroinformatics (2014), 8.

[37] S.W. Keemink, S.C. Lowe, J.M.P. Pakan, E. Dylda, M.C.W. van Rossum, N. L. Rochefort, FISSA: a neuropil decontamination toolbox for calcium imaging signals, Sci Rep. 8 (February 22 (1)) (2018) 3493.
[38] T.-W. Chen, T.J. Wardill, Y. Sun, S.R. Pulver, S.L. Renninger, A. Baohan, et al., Ultra-sensitive fluorescent proteins for imaging neuronal activity, Nature 499 (July 18 (7458)) (2013) 295–300.
[39] M. Kirkcaldie, C. Watson, G. Paxinos, K. Franklin, Straightening Out the Mouse Neocortex, 2012, p. 1.
[40] H. Tsukano, M. Horie, T. Bo, A. Uchimura, R. Hishida, M. Kudoh, et al., Delineation of a frequency-organized region isolated from the mouse primary auditory cortex, J. Neurophysiol. 113 (April (7)) (2015) 2900–2920.
[41] I. Stiebler, R. Neulist, I. Fichtel, G. Ehret, The auditory cortex of the house mouse: left-right differences, tonotopic organization and quantitative analysis of frequency representation, J. Comp. Physiol. A 181 (December 1(6)) (1997) 559–571.
[42] A. Nelson, R. Mooney, The basal forebrain and motor cortex provide convergent yet distinct movement-related inputs to the auditory cortex, Neuron 90 (May 4 (3)) (2016) 635–648.
[43] D.M. Schneider, J. Sundararajan, R. Mooney, A cortical filter that learns to suppress the acoustic consequences of movement, Nature 561 (September (7723)) (2018) 391–395.
[44] F. Barthas, A.C. Kwan, Secondary motor cortex: where 'Sensory' meets 'Motor' in the rodent frontal cortex, Trends Neurosci. 40 (March (3)) (2017) 181–193.
[45] H. Markram, M. Toledo-Rodriguez, Y. Wang, A. Gupta, G. Silberberg, C. Wu, Interneurons of the neocortical inhibitory system, Nat. Rev. Neurosci. 5 (October (10)) (2004) 793–807.
[46] N. Tamamaki, Y. Yanagawa, R. Tomioka, J.-I. Miyazaki, K. Obata, T. Kaneko, Green fluorescent protein expression and colocalization with calretinin, parvalbumin, and somatostatin in the GAD67-GFP knock-in mouse, J. Comp. Neurol. 467 (December 1 (1)) (2003) 60–79.
[47] R. Tomioka, K. Okamoto, T. Furuta, F. Fujiyama, T. Iwasato, Y. Yanagawa, et al., Demonstration of long-range GABAergic connections distributed throughout the mouse neocortex, Eur. J. Neurosci. 21 (March (6)) (2005) 1587–1600.
[48] K. Yuan, K.L. Fink, J.A. Winer, C.E. Schreiner, Local connection patterns of parvalbumin-positive inhibitory interneurons in rat primary auditory cortex, Hear Res 274 (2011).
[49] J. Reimer, E. Froudarakis, C.R. Cadwell, D. Yatsenko, G.H. Denfield, A.S. Tolias, Pupil fluctuations track fast switching of cortical states during quiet wakefulness, Neuron 84 (October 22 (2)) (2014) 355–362.
[50] M. Vinck, R. Batista-Brito, U. Knoblich, J.A. Cardin, Arousal and locomotion make distinct contributions to cortical activity patterns and visual encoding, Neuron 86 (May 6 (3)) (2015) 740–754.
[51] D.A. Dombeck, A.N. Khabbaz, F. Collman, T.L. Adelman, D.W. Tank, Imaging large-scale neural activity with cellular resolution in awake, mobile mice, Neuron 56 (October 4 (1)) (2007) 43–57.
[52] C. Grienberger, A. Konnerth, Imaging calcium in neurons, Neuron 73 (March 8 (5)) (2012) 862–885.
[53] M.J. McGinley, S.V. David, D.A. McCormick, Cortical membrane potential signature of optimal states for sensory signal detection, Neuron 87 (July 1 (1)) (2015) 179–192.
[54] S.O. Aliu, J.F. Houde, S.S. Nagarajan, Motor-induced suppression of the auditory cortex, J. Cogn. Neurosci. 21 (July 1 (4)) (2008) 791–802.
[55] M.H. Martikainen, K. Kaneko, R. Hari, Suppressed responses to self-triggered sounds in the human auditory cortex, Cereb. Cortex 15 (March 1 (3)) (2005) 299–302.
[56] N.G. Mifsud, L.K.L. Oestreich, B.N. Jack, J.M. Ford, B.J. Roach, D.H. Mathalon, et al., Self-initiated actions result in suppressed auditory but amplified visual evoked components in healthy participants, Psychophysiology 53 (5) (2016) 723–732.
[57] A. Flinker, E.F. Chang, H.E. Kirsch, N.M. Barbaro, N.E. Crone, R.T. Knight, Single-trial speech suppression of auditory cortex activity in humans, J. Neurosci. Off. J. Soc. Neurosci. 30 (December 8 (49)) (2010) 16643–16650.
[58] M. Dipoppa, A. Ranson, M. Krumin, M. Pachitariu, M. Carandini, K.D. Harris, Vision and locomotion shape the interactions between neuron types in mouse visual cortex, Neuron 98 (May 2 (3)) (2018) 602–615.e8.
[59] Y. Fu, J.M. Tucciarone, J.S. Espinosa, N. Sheng, D.P. Darcy, R.A. Nicoll, et al., A cortical circuit for gain control by behavioral state, Cell 156 (March 13 (6)) (2014) 1139–1152.
[60] P.-O. Polack, J. Friedman, P. Golshani, Cellular mechanisms of brain state–dependent gain modulation in visual cortex, Nat. Neurosci. 16 (September (9)) (2013) 1331–1339.
[61] W. Guo, A.R. Chambers, K.N. Darrow, K.E. Hancock, B.G. Shinn-Cunningham, D. B. Polley, Robustness of cortical topography across fields, laminae, Anesthetic States, and neurophysiological signal types, J. Neurosci. 32 (July 4 (27)) (2012) 9159–9172.
[62] S. Romero, A.E. Hight, K.K. Clayton, J. Resnik, R.S. Williamson, K.E. Hancock, et al., Cellular and widefield imaging of sound frequency organization in primary and higher order fields of the mouse auditory cortex, Cereb Cortex N Y N 1991 30 (March 14 (3)) (2020) 1603–1622.
[63] F. Liang, H. Li, X. Chou, M. Zhou, N.K. Zhang, Z. Xiao, et al., Sparse representation in awake auditory cortex: cell-type dependence, synaptic mechanisms, developmental emergence, and modulation, Cereb. Cortex 29 (August 14 (9)) (2019) 3796–3812.
[64] J. He, T. Hashikawa, H. Ojima, Y. Kinouchi, Temporal integration and duration tuning in the dorsal zone of cat auditory cortex, J. Neurosci. 17 (April 1 (7)) (1997) 2615–2625.
[65] G.C. Stecker, I.A. Harrington, E.A. Macpherson, J.C. Middlebrooks, Spatial sensitivity in the Dorsal Zone (Area DZ) of cat auditory cortex, J. Neurophysiol. 94 (August 1 (2)) (2005) 1267–1280.
[66] P. Kusmierek, J.P. Rauschecker, Selectivity for space and time in early areas of the auditory dorsal stream in the rhesus monkey, J. Neurophysiol. 111 (April (8)) (2014) 1671–1685.
[67] G.H. Recanzone, Spatial processing in the auditory cortex of the macaque monkey, Proc. Natl. Acad. Sci. 97 (October 24 (22)) (2000) 11829–11835.
[68] B. Tian, D. Reser, A. Durham, A. Kustov, J.P. Rauschecker, Functional specialization in rhesus monkey auditory cortex, Science 292 (April 13 (5515)) (2001) 290–293.
[69] N.H. Salminen, H. Tiitinen, P.J.C. May, Auditory spatial processing in the human cortex, Neuroscientist 18 (December 1 (6)) (2012) 602–612.
[70] J. Liu, M.R. Whiteway, A. Sheikhattar, D.A. Butts, B. Babadi, P.O. Kanold, Parallel processing of sound dynamics across mouse auditory cortex via spatially patterned thalamic inputs and distinct areal intracortical circuits, Cell Rep. 27 (April (3)) (2019) 872–885.e7.
[71] M. Manto, J.M. Bower, A.B. Conforto, J.M. Delgado-García, S.N.F. da Guarda, M. Gerwig, et al., Consensus paper: roles of the cerebellum in motor control—the diversity of ideas on cerebellar involvement in movement, Cerebellum Lond Engl. 11 (June (2)) (2012) 457–487.
[72] O. Baumann, J.B. Mattingley, Scaling of neural responses to visual and auditory motion in the human cerebellum, J. Neurosci. 30 (March 24 (12)) (2010) 4489–4495.
[73] N.M. McLachlan, S.J. Wilson, The contribution of brainstem and cerebellar pathways to auditory recognition, Front Psychol. (March 20) (2017) 8.
[74] A. Petacchi, A.R. Laird, P.T. Fox, J.M. Bower, Cerebellum and auditory function: an ALE meta-analysis of functional neuroimaging studies, Hum. Brain Mapp. 25 (May (1)) (2005) 118–128.
[75] L.S. Popa, T.J. Ebner, Cerebellum, predictions and errors, Front. Cell. Neurosci. 12 (2018) 524.
[76] K.V. Kuchibhotla, J.V. Gill, G.W. Lindsay, E.S. Papadoyannis, R.E. Field, T. A. Hindmarsh Sten, et al., Parallel processing by cortical inhibition enables context-dependent behavior, Nat. Neurosci. 20 (January (1)) (2017) 62–71.
[77] K.K. Clayton, R.S. Williamson, K.E. Hancock, G. Tasaka, A. Mizrahi, T.A. Hackett, et al., Auditory corticothalamic neurons are recruited by motor preparatory inputs, Curr. Biol. 31 (January 25 (2)) (2021) 310–321.e5.
[78] V.V. Stoilova, B. Knauer, S. Berg, E. Rieber, F. Jäkel, M.C. Stüttgen, Auditory cortex reflects goal-directed movement but is not necessary for behavioral adaptation in sound-cued reward tracking, J. Neurophysiol. 124 (August 26 (4)) (2020) 1056–1071.
[79] K.A. Ferguson, J.A. Cardin, Mechanisms underlying gain modulation in the cortex, Nat Rev Neurosci. 21 (February (2)) (2020) 80–92.
[80] J.S. Isaacson, M. Scanziani, How inhibition shapes cortical activity, Neuron 72 (October 20 (2)) (2011) 231–243.
[81] P.O. Kanold, I. Nelken, D.B. Polley, Local versus global scales of organization in auditory cortex, Trends Neurosci. 37 (September (9)) (2014) 502–510.
[82] C.K. Pfeffer, M. Xue, M. He, Z.J. Huang, M. Scanziani, Inhibition of inhibition in visual cortex: the logic of connections between molecularly distinct interneurons, Nat. Neurosci. 16 (August (8)) (2013) 1068–1076.
[83] J. Jackson, I. Ayzenshtat, M.M. Karnani, R. Yuste, VIP+ interneurons control neocortical activity across brain states, J. Neurophysiol. 115 (June 1 (6)) (2016) 3008–3017.
[84] S. Lee, I. Kruglikov, Z.J. Huang, G. Fishell, B. Rudy, A disinhibitory circuit mediates motor integration in the somatosensory cortex, Nat. Neurosci. 16 (November (11)) (2013) 1662–1670.
[85] H.-J. Pi, B. Hangya, D. Kvitsiani, J.I. Sanders, Z.J. Huang, A. Kepecs, Cortical interneurons that specialize in disinhibitory control, Nature 503 (November (7477)) (2013) 521–524.
[86] L. Mesik, W. Ma, L. Li, L.A. Ibrahim, Z.J. Huang, L.I. Zhang, et al., Functional response properties of VIP-expressing inhibitory neurons in mouse visual and auditory cortex, Front Neural Circuits (2015) 9.
[87] B. Rudy, G. Fishell, S. Lee, J. Hjerling-Leffler, Three groups of interneurons account for nearly 100% of neocortical GABAergic neurons, Dev. Neurobiol. 71 (1) (2011) 45–61.